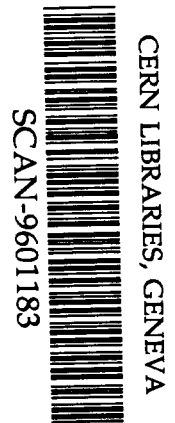


**Operation and performance of the
Cosmic Ray Tracking detector system**

K. Bernlöhr, W. Hofmann, G. Leffers, V. Matheis,
M. Panter, U. Trunk, M. Ulrich, T. Wolf, R. Zink

Max-Planck-Institut für Kernphysik
Postfach 103980, D-69029 Heidelberg, Germany

MPIK - V 31 - 1995



SU 9.505

Operation and performance of the Cosmic Ray Tracking detector system

K. Bernlöhner, W. Hofmann, G. Leffers, V. Matheis,
M. Panter, U. Trunk, M. Ulrich, T. Wolf, R. Zink
Max-Planck-Institut für Kernphysik, Heidelberg, Germany

July 12, 1995

Abstract

The Cosmic Ray Tracking (CRT) project represents a study on the use of tracking detectors of the time projection chamber type to detect secondary cosmic ray particles in extensive air showers. The concepts of an array of CRT detectors and the detector hardware, including the custom-designed electronics, are described in a preceding article.

A CRT detector consists of two circular drift chambers of 1.8 m diameter with six sense wires each, and a 10 cm thick iron plate as a muon filter between the two chambers. Each detector has a local electronics box with a readout, trigger, and monitoring system. The local computers at the detector stations are used for hit and track finding in parallel to the detector readout. Detector stations are permanently calibrated online, using the cosmic ray data. The online software, including data processing and calibration procedures, are presented in this paper. Ten detectors are in operation at the site of the HEGRA air shower array. The detector performance has been evaluated using data from these detectors and the HEGRA array as well as by Monte Carlo simulations.

The spatial resolution has been found to be about 1 mm both in drift and in wire direction. The corresponding angular resolution is about 0.4° in each projection for a single track. Muons are usually identified if scattered by less than 2.5° in the iron plate, corresponding to energies of more than about 1 GeV. In HEGRA-triggered showers an overall muon identification efficiency of 87% is achieved, with a fraction of only 0.07% of the electrons being misidentified as muons.

1 Introduction

Cosmic rays of very high energies - of the order of TeV and above - give rise to *extensive air showers* (EAS) where charged secondary particles may reach ground-level. The traditional detection technique for EAS is that of scintillator arrays which reconstruct the shower direction from the differences of arrival times of secondary particles in counters separated by tens to hundreds of meters (timing method). In the *Cosmic Ray Tracking* (CRT) project, detectors have been developed to reconstruct shower directions from the arrival directions of the

secondaries (tracking method). Tracking detectors make use of the angular correlation of secondaries with primary cosmic rays. Most charged secondaries in an EAS are electrons or positrons and arrive typically within a few degrees from the direction of the primary. Muons in EAS are even better correlated with the primary. In electromagnetic showers, muons are more than an order of magnitude less abundant than in hadronic showers caused by protons and nuclei. Selecting muon-poor showers is the most powerful method for air shower arrays to suppress the strong hadronic background when searching for sources of *very-high-energy* (VHE) γ -rays.

The CRT project has been initiated in 1988 by proposing an array of almost 400 tracking detectors with muon identification [1, 2, 3]. Such a CRT array would achieve a lower energy threshold than any existing particle detector array (about 3 TeV at an altitude near 4000 m). Its main purpose would be to search for γ -ray sources.

The detectors, that have been developed, use two circular drift chambers of the *time projection chamber* (TPC) type and a 10 cm thick iron plate as muon filter between the two chambers. Drift chambers and iron plate have a diameter of 1.8 m. Each detector has a local computer for readout of the FADC system, for track reconstruction, and detector calibration. Ten CRT detectors are in operation at the site of the HEGRA experiment [12] on La Palma, Canary Islands, for up to two years. Detector hardware and the custom-designed electronics are described in detail in another paper [4] (in the following referred to as Paper I). The main purposes of this installation have been long-term operation tests at mountain-altitude conditions and the evaluation of the detector performance under such conditions. The angular resolution and the hadron rejection of this mini-array of 10 detectors are not considered to be sufficient to search for steady γ -ray sources but are appropriate to check for VHE γ -rays from known *gamma-ray bursts* (GRB) [5].

The CRT detectors on La Palma have been operated with online hit finding, track reconstruction, and detector calibration, as intended for a large CRT array. With such data processing at the detector stations, only the track data has to be transferred to a central computer system for further processing, like shower reconstruction, and for tape backup. Otherwise, the data rates and required processing power for a central station would be excessive. In the following section the online software including local data processing at the detector stations is described. The online calibration procedures as well as dedicated detector test setups are explained thereafter. A detailed Monte Carlo simulation of the CRT detectors is used to check our understanding of the detector and to evaluate performance parameters which cannot be easily measured. Finally, the performance of the detectors on La Palma is presented.

2 The online software

2.1 Design goals

In the design of the CRT online software, several requirements had to be met. With as many detectors as proposed for a full-sized CRT array, the local detector

stations have to be independent, requiring little central control, and, in particular, very little control by personal during regular operation. Dead-time caused by calibration tasks should be small.

The Motorola 68040 processor provides enough computing power for local data processing at each detector station. This processing includes hit finding and track reconstruction. During regular operation, only track data should be transmitted to the central computer. For offline testing and optimizing of the processing algorithms the data from preceding processing stages can be transmitted as well. Since different kinds of computers are used for offline data analysis, a hardware-independent data format is used. The whole online software has been ported to different kinds of realtime operating systems, like OS-9 and Lynx-OS. An array of CRT stations could even be operated in a mixed operating system environment.

The main tasks for central online computers in the array remain network communication, event building, and shower reconstruction from the particle tracks reconstructed at the detector stations.

2.2 Data readout of the detectors

A multi-buffer scheme is used for the FADC event data readout of the detectors. The actual readout is implemented as an interrupt service function (separate process thread) filling raw data buffers in the computer main memory, as long as a free buffer is available. These raw data buffers are processed and released later by the main online task. Typically, buffers for 15 events are used. Therefore, the online data processing causes essentially no additional dead-time, as long as the average trigger rate is below the average rate at which events can be processed.

The readout interrupt is initiated either by the FADC Master module or by the Event Grader module, depending on the trigger conditions. When the CRT detectors are operated as part of an array ('array' or 'external trigger' mode of operation), the trigger signal and the CPU interrupt are generated by the Event Grader module. When the CRT detector is operated independent of others ('stand-alone' or 'internal trigger' mode), trigger signals are generated by the trigger module and CPU interrupts by the FADC Master.

In the interrupt service function a fast scan of the wire channels is done to look for data sections of interest. With each 32-bit VME-bus access, data from four different FADC channels are read. For a pulse length of more than 200 ns, it is sufficient to inspect only every 5th word. Because the nominal FADC pedestal (baseline) is set a few counts below a threshold at a power of 2 (e.g. a baseline at 12 for a threshold at 16), only a simple comparison with a bit mask is required to see if any of the four channels is above the threshold. If so, the wire data and the corresponding cathode pad data are copied from FADC memory to main memory until all four wire channels are below threshold again. Reasonable prefix and postfix regions are included in each such data section. After the complete readout, the FADC system is restarted. In external trigger mode, the EGS (*Event Grader Slave*, see paper I) is also enabled again.

2.3 Hit finding

At first, the main online task searches for hits in the wire raw data (see fig. 1). For a charge-division wire the average of both ends is used. The *difference-of-samples* (DOS) method is applied for finding hits. The difference of the contents in consecutive bins is required to exceed a given threshold. The signal itself also has to exceed a threshold above the nominal baseline value for several bins in sequence, in order to reject noise. The start time of a pulse is defined by a weighted centre of the difference signal in the rising part of the pulse. A good identification of overlapping pulses is achieved by the DOS method for separations of more than about one full-width at half maximum (FWHM) of a pulse (about 200 ns).

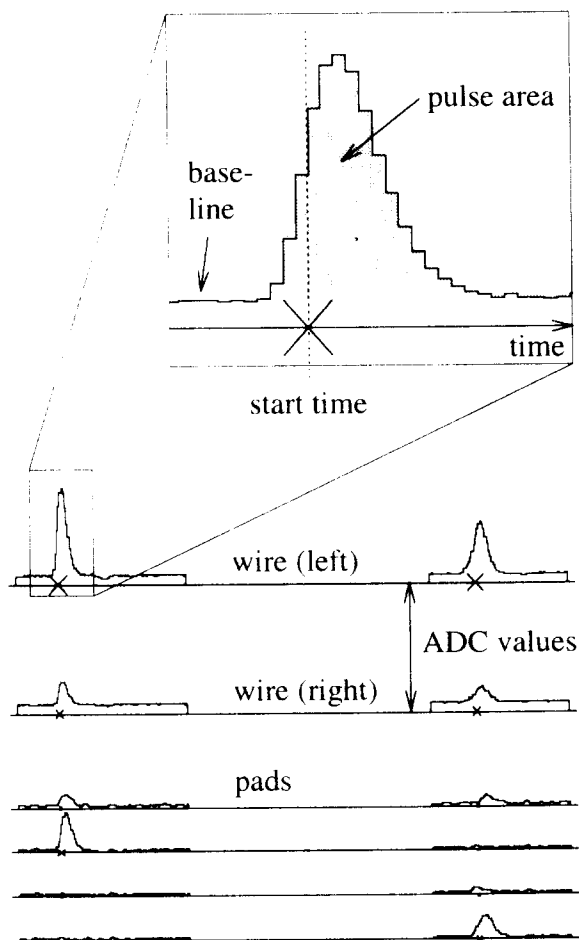


Figure 1: FADC raw data and two identified hits shown for both sides of a charge-division wire and the corresponding four cathode pads. The data corresponds to a time interval of about $9 \mu\text{s}$. Positions and sizes of crosses indicate the reconstructed start times and pulse areas, respectively.

For the reconstruction of coordinates along the wires, ratios of charges on the two ends of charge-division wires or on the four pad channels, respectively, are of importance. The *pulse areas* which measure these charges have to be determined in a way which optimizes signal-to-noise of the relevant ratios. For this reason,

the number of bins contributing to a pulse area varies slightly with the size of the pulse. As a consequence, pulse areas are not strictly proportional to the charges. As long as the same bins are used for all channels involved in a ratio, the ratio of charges remains proportional to the ratio of pulse areas. Similarly, if a bin is in overflow for one channel, it is discarded for all participating channels. In overlapping pulses, the tails of the earlier pulses are subtracted from the later pulses (for details see [6]).

2.4 Track finding and reconstruction

The drift times are available for hits on all six wires of a drift chamber – except for a common trigger offset t_0 – whereas the positions in wire direction can be reconstructed only on two charge-division wires without ambiguities. Therefore, the track finding is based entirely on the drift times. The x (drift) coordinates of the hits are evaluated for both sides of the wire ‘plane’, given the measured time $t - t_0$, the drift velocity v_d , and the wire staggering x_w :

$$x_{\pm} = x_w \pm v_d(t - t_0).$$

Track candidates are searched along straight lines through suitable pairs of hits on two *seed wires*. Projected zenith angles of less than 60° are required. On the other four wires, hits less than 8 mm from that line are accepted. This search is done under both assumptions that the track is on either side of the wire plane. If suitable hits are found on enough wires, least squares fits are applied, which resolve the x_{\pm} ambiguity by using the side with the smaller χ^2 per *number of degrees of freedom* (ndf). Track candidates with a bad χ^2/ndf are discarded. While the 8-mm cut is rather loose in events with few track candidates in a chamber, it is tightened for events with many candidates to reduce the risk of having random combinations of hits misidentified as tracks. Track candidates are required to have hits on at least four wires. To have full efficiency, three different pairs of seed wires are used as starting points for this track search.

Most tracks are found from more than one pair of seed wires and different tracks may have one or more common hits. A hit common to two tracks is removed from the track with the larger residual of this hit, if the difference is significant, or from the track with the worse χ^2/ndf . Tracks with too few remaining hits are discarded, otherwise the least squares fit is repeated. In the end, no hit is assigned to more than one track.

For the remaining tracks, the y (wire) coordinates and slopes are evaluated, provided that the tracks have at least hits on both charge-division wires or on one charge-division wire and one other wire with cathode pads. The charge-division coordinates y_{cd} are obtained from the charges q_r and q_l measured on the right and left sides of the wires (see section 3.5). The y_{cd} coordinates are required to resolve the 22-fold ambiguity of the more precise pad coordinates y_{pad} . The pad coordinates are derived from the centre-of-gravity of the pad with the largest charge and its two neighbours and then corrected for remaining systematic errors via a lookup table (see section 3.4).

If hits on both charge-division wires are available, a straight line through the combined y positions is extrapolated to the other wire(s) with pads. There, the

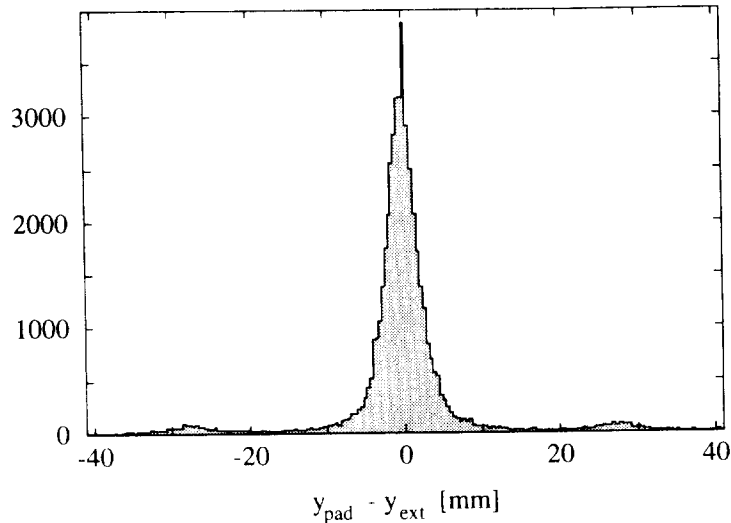


Figure 2: Offsets of pad coordinates y_{pad} on a non-charge-division wire from the extrapolation y_{ext} from the charge-division wires in events with one track only. The small peaks at ± 28 mm arise from tracks where a charge-division coordinate is wrong by more than half of a pad period.

extrapolated positions y_{ext} are used to resolve the pad ambiguity (see fig. 2). A least squares track fit is applied to the set of all available y coordinates from charge-division and non-charge-division wires with pads. If on the non-charge-division wire(s) the y_{ext} (modulo the pad period length) are not in reasonable agreement with the derived pad coordinates, one or both of the charge-division coordinates may be wrong. In such a case, the wire causing the problem is usually identified, e.g. by an overflow, a very small signal, or overlapping pulses, and the correct s_y track slope is derived without the signals of this wire. If only hits on one charge-division wire and on one other wire with pads are available, some ambiguity of the track slope remains.

Finally, corrections for small angular and spatial misalignments of the two drift chambers of a detector (see sect. 3.6) have to be applied before muons can be identified.

2.5 Muon identification

The identification of muons was an important aspect in the design of the CRT detectors. After the track reconstruction, muon identification is a further step of the data processing which can be done online at individual detector stations. For this purpose, all pairs of one track in the upper chamber and one in the lower chamber are compared. Both slope components should be consistent. Due to the 90° rotation angle between upper and lower chambers this can be written as

$$s_{x,u} \approx s_{y,l} \quad (1)$$

$$s_{y,u} \approx -s_{x,l} \quad (2)$$

for the slope components in x and y projection of the tracks in the upper and lower chamber, respectively, with x always being measured in drift direction of a drift chamber, y in wire direction.

An additional condition is that the tracks in the upper and lower chambers match when they are extrapolated to the middle of the iron plate: $x_u \approx y_l$, $y_u \approx -x_l$. However, the delay between the particle arrival time and the FADC stop signal is not well known, i.e. the x coordinates have a common but event-dependent offset. There is one linear combination of the intersection coordinates, $\rho_1 = (x_u \pm y_l) \pm (x_l \pm y_u)$, which is independent of this offset, with signs depending on the ‘quadrant’ (the combination of the drift cages in the two drift chambers). If the offset is known, the orthogonal linear combination ρ_2 can be used to check that a muon candidate arrived at the proper time:

$$\rho_1 \approx 0 \tag{3}$$

$$\rho_2 - v_d t_0 \approx 0. \tag{4}$$

Indeed, muons unrelated with the showers triggering the array of CRT detectors are expected to be the most severe background to muons of the showers, if the trigger delay is not known. It is usually not known during online pattern recognition at a detector station but can be determined in the case of a CRT array triggered by CRT detectors only, after combining data from many detectors at the central station. In the case of the detectors triggered by the HEGRA scintillator array, the trigger delay is well known.

Other possible sources of muon background are hadrons and punch-through electrons. Charged high-energy hadrons are likely to be misidentified as muons because the iron plate has a thickness of only 0.6 interaction lengths. For a search for γ -ray sources misidentified hadrons are of no concern because they, like muons, are indicators of nucleon-induced air showers. In addition, charged high-energy hadrons are only found very close to the shower axis. Electrons of more than about 1 GeV energy, also found only close to the shower axis, may give rise to electromagnetic showers in the iron plate, with opening angles of secondaries in the lower drift chamber of several ten degrees. Such muon background can be easily rejected by applying isolation criteria to the ‘muon’ track in the lower chamber. Real ‘punch-through’ electrons with a single track in the lower chamber within a 2° cone of the upper track are very unlikely and not a severe muon background (see sects. 4 and 5.4).

2.6 Tasks of the central VME system

Two computers are used at the central station: a VME system for the control of common triggers and common event numbers in array mode and an UNIX workstation for collecting event data, event building, online shower reconstruction, and data backup. For the central VME system a Motorola 68040 CPU is currently used.

The central VME system is used to control the central trigger electronics and the Event Grader Master. In the setup on La Palma, the VDIO and Clock modules for cross-references to the HEGRA data are also included in this central system.

The Event Grader Master module sends the trigger plus 16-bit event number for each accepted central trigger and generates an interrupt. The central trigger is also used to store the precise time in the Clock module latch registers.

The interrupt handler function obtains the 16-bit HEGRA event number from the VDIO module and the stored time from the Clock module, increments the current event number and stores the lower 16 bits of the new number in the Event Grader Master module for the next trigger. Whenever the upper bits of the event number change, they are distributed to all detector stations. Finally, the electronics is enabled for the next event.

2.7 Communication and event building

The event numbers are used for event building in the central computer when the asynchronously processed data from all detector modules are collected there. In the initial test phase with CRT detectors, the data from each detector was written to a separate file and the event building was done offline.

Remote detector control and data transfer are implemented on top of the connectionless *User Datagram Protocol* (UDP) to achieve high transfer rates via Ethernet. Remote control of the data acquisition program at the detector modules, of the run control program at the central VME system, and of the event builder and I/O server program at the UNIX workstation is possible from different types of UNIX workstations and also from VMS or OS-9 systems connected to the local network.

Diagnostic and calibration histograms from any CRT station are available online for remote inspection. The central VME system communicates with the UNIX system as well as with all involved detector module computers for starting and stopping runs. The detector computers also communicate with the UNIX system for assigning output files, for data transfer, clock synchronization, and problem reports.

Data are collected by the detector computers until a given block limit (typically 64 kbytes) is reached, the data are requested by the central station, or a run is stopped.

3 Detector calibration

3.1 Online calibration stages

The online calibration procedure consists of four stages which are carried out continuously during regular data acquisition. Except for the first stage, the FADC baseline calibration, all calibration stages use regular event data. Therefore, periodic updating of all relevant parameters on a short time-scale is achieved essentially without interrupting the data acquisition. Only the baseline calibration, which is repeated every few hundred events, gives rise to short dead-time intervals. The later stages can also be performed offline if raw data or hit data are recorded.

Each calibration stage, except for the baseline calibration, requires that the preceding stage has been passed at least once. Apart from that, data for the different stage are collected independently and in parallel. When enough data

are accumulated for a stage, the corresponding parameters are determined and updated. Changes of calibration parameters are usually recorded just like event data. The calibration status can be saved when a run is terminated and restored before the next run is started. Otherwise, after starting with an uncalibrated detector, some 30000 self-triggered events are required for a complete pass through all stages, which takes about 10 minutes.

3.2 FADC baseline calibration

The recorded FADC baselines or pedestals change with the offset of the shaper outputs and depend on the temperature in the electronics box. The temperature dependence is generally less than 0.2 FADC counts per Kelvin but has to be taken into account for an accurate reconstruction of pulse areas.

The FADC baselines are monitored at regular intervals by reading all 2048 bins of each FADC channel and computing the average values after checking that there are no random pulses in the data. For the reconstruction of pulse areas this measured FADC baseline is used, not the nominal value. If the measured baseline of any channel deviates from the nominal value by more than 0.5 counts, the baseline is adjusted by changing the DAC setting of that FADC channel and measuring the baseline again.

3.3 Gain calibration

The average ratio of pulse areas to the number of electrons drifting to a wire, depends mainly on the gas amplification g_{gas} , the gains g_e of preamplifiers and shapers, and the sensitivity s_{adc} of the FADCs. For the reconstruction of particle tracks with the CRT detectors, it is important to know the ratios of the overall gains of both sides of the charge-division wires and of all four channels of the pad boards. The absolute value of the overall gain, on the other hand, is of minor importance and does not need permanent monitoring. The temperature dependence of the gas amplification is common to all readout channels of a wire and has no impact on the track reconstruction. An arbitrary scale factor A common to all relevant readout channels of a wire can be included in the calibration of ‘charges’ q from the measured FADC pulse areas P :

$$q = \frac{A}{g_{\text{gas}}g_e s_{\text{adc}}} P = c P. \quad (5)$$

A single calibration factor c for each readout channel is thus sufficient.

Gain variations of the electronic chain can be monitored with test pulses from the fast DAC on the monitor module or an external pulser connected to the test inputs of all preamplifiers. Monitoring of the electronic gain variations was important in finding out the characteristic amplitudes and time scales of gain-ratio variations of separate channels. In practice, amplitudes of such variations are small enough and time scales large enough that test pulses are not required during regular detector operation.

Instead, the regular monitoring is done with the cosmic-ray data, using pulse-area histograms of all input channels (see fig. 3). For wire channels the calibration

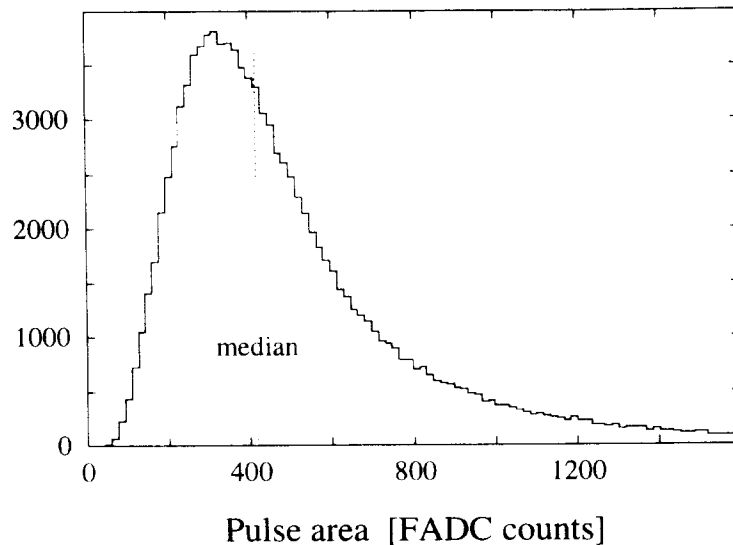


Figure 3: Histogram of wire pulse areas. The gain calibration is derived from the median value.

constants c are obtained from the median pulse area values including overflow pulses. For pad channels, on the other hand, those values where 75% of all histogram entries have smaller pulse areas turned out to be more appropriate. After a sufficient number – typically 5000 – isolated hits are recorded for each wire of a drift chamber, the calibration values are obtained from the histograms and the histogram contents are reset. Up to 10 successive values are stored for each input channel and the actual calibration constant is obtained from a straight line fit to these values, extrapolated to the middle of the next calibration interval to account for gradual changes with time.

3.4 Coordinates derived from cathode-pad signals

The *centre-of-gravity* (c.o.g.) method for reconstructing the pad coordinate from the ‘charge’ q_i of the cathode pad i with the largest signal and those of its two neighbours, q_{i-1} and q_{i+1} , is used as a first approximation:

$$y_{c.o.g.} = \frac{q_{i+1} - q_{i-1}}{q_{i+1} + q_i + q_{i-1}} l_p + y_i, \quad (6)$$

where l_p is the length of the pads (20.5 mm) and y_i is the position of the middle of pad i .

With the pad spacing used for CRT, systematic imaging errors of up to $\pm 4\%$ of the pad length (0.9 mm) would result by using the c.o.g. method alone. Hits are preferentially reconstructed near the centre of a pad (fig. 4a). An additional correction is required to achieve the inherent resolution. This correction is based on the fact that the true pad coordinate y_{pad} is a strictly monotonic function of the c.o.g. coordinate $y_{c.o.g.}$ and that, averaged over all 88 pads on a board, any position between $-l_p/2$ and $+l_p/2$ along the pad of length l_p has essentially the same probability.

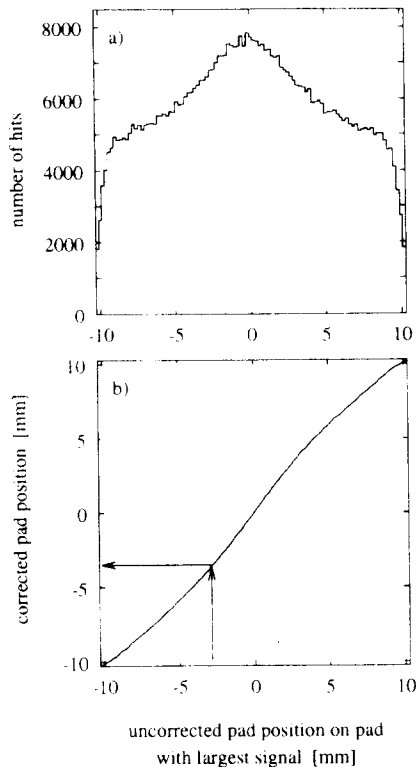


Figure 4: a) Histogram of uncorrected pad coordinates $y_{c.o.g.}$. b) Lookup table for $y_{pad}(y_{c.o.g.})$.

If the probability of measuring $y_{c.o.g.}$ is $p(y_{c.o.g.})$, the corresponding strictly monotonic function of $y_{c.o.g.}$ with constant probability within $-l_p/2$ to $+l_p/2$ is obtained from

$$y_{pad}(y_{c.o.g.}) = l_p \left(\frac{\int_{-l_p/2}^{y_{c.o.g.}} p(y) dy}{\int_{-l_p/2}^{l_p/2} p(y) dy - 0.5} \right). \quad (7)$$

For CRT, a lookup table for the correction of the pad coordinates (fig. 4b) is obtained from a histogram of $p(y_{c.o.g.})$ (fig. 4a), which is integrated bin by bin and normalized. Linear interpolation between neighbouring bins is used for each coordinate lookup.

3.5 Charge-division calibration

Even with a perfect charge-division readout system and a perfect gain calibration a further calibration constant, the *effective length* l_{eff} , is required for reconstructing coordinates y_{cd} along a wire:

$$y_{cd} = \frac{l_{eff}}{2} \frac{q_r - q_l}{q_r + q_l} = \frac{l_{eff}}{2} r_{cd}, \quad (8)$$

with the gain-calibrated ‘charges’ $q_r = c_r P_r$ and $q_l = c_l P_l$ from the ‘right’ and ‘left’ sides of the wire, respectively. For equal input resistances R_{in} of the preamplifiers on both sides and wire resistance R_w , the effective length is related to the wire length l by

$$l_{\text{eff}} = l \left(1 + \frac{2R_{in}}{R_w} \right). \quad (9)$$

In a real-world detector, there are not only differences in the gains of the two readout channels of a charge-division wire but also in the input resistances of the two preamplifiers. As a consequence, eq. 8 is only an approximation. For known input and wire resistances, the required corrections could be calculated exactly. In practice, a polynomial approximation of order 2 is sufficient:

$$y_{\text{cd}} = a_0 + a_1 r_{\text{cd}} + a_2 r_{\text{cd}}^2, \quad (10)$$

with

$$r_{\text{cd}} = (c_r P_r - c_l P_l) / (c_r P_r + c_l P_l). \quad (11)$$

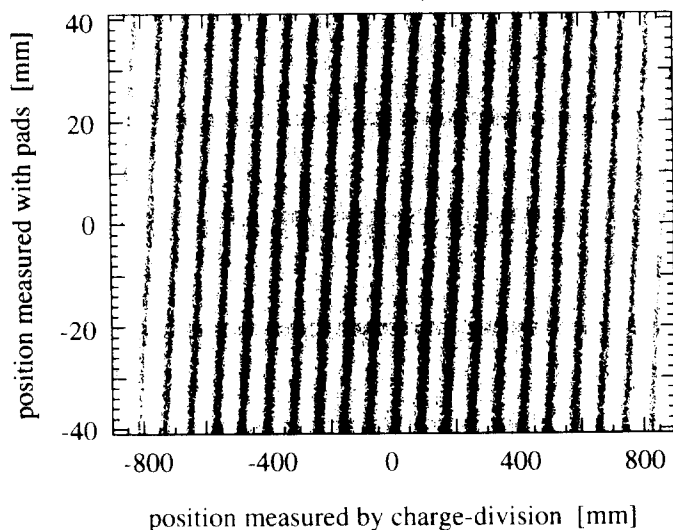


Figure 5: Histogram of charge-division and pad coordinates.

The coefficients of such a polynomial are obtained by comparing charge-division and pad coordinates for many hits (see fig. 5). The pad period lengths $l_{\text{pp}} = 4l_{\text{p}}$ can be measured with an accuracy of about 0.03 mm before the installation, and significant misalignments – larger than the usual installation tolerance of 0.1 mm – would be visible in the average residuals of the track fits. Due to the ambiguity of the coordinates y_{pad} derived from the pad signals, the relation

$$y_{\text{cd}} \approx y_{\text{pad}} + \bar{y}_j \quad (j = 1, \dots, n_{\text{pp}}) \quad (12)$$

has to be used, where \bar{y}_j is the coordinate of the centre of the unknown pad period j where the signal was actually induced:

$$\bar{y}_j = (j - n_{\text{pad}}/2 - 0.5) l_{\text{pp}}. \quad (13)$$

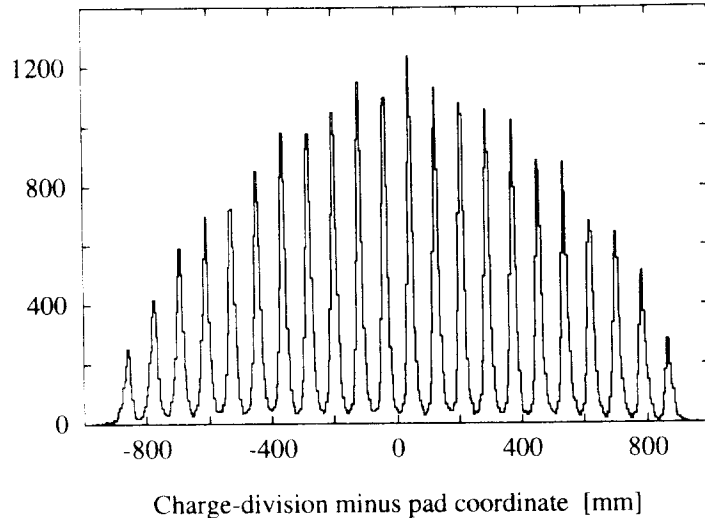


Figure 6: Histogram of $y_{cd} - y_{pad}$ as used for the calibration of the charge-division.

Therefore, histograms of $y_{cd} - y_{pad}$ show as many peaks as there are pad periods, $n_{pp} = 22$ (fig. 6). To determine a new set of a_0 , a_1 , and a_2 , each measured peak position is first transformed to a corresponding r_{cd} , using the previous set of calibration constants, and then a parabola is fitted to the 22 expected positions versus the measured r_{cd} ratios.

The widths of the peaks are dominated by the average charge-division resolution at the corresponding pad period because the statistical errors of the pad coordinates are small compared to those of the charge-division. The widths are smallest near the middle of the wire ($\sigma_{cd} \approx 9$ mm) and increase by about a factor of $\sqrt{2}$ towards the ends, as to be expected from eq. 8.

3.6 Drift velocity and alignment

Due to the 90° rotation between the two drift chambers of a CRT detector the drift velocity v can be easily calibrated with cosmic-ray muons. Muons of more than 140 MeV kinetic energy pass through the iron plate and muons of more than 1 GeV are scattered on average by less than 2° . For such an almost straight muon track the slope in drift direction of one chamber $s_x = \tan \theta_x$, where θ_x is the projected zenith angle, should be the same as that in wire direction (s_y) of the other chamber and vice versa. What is actually measured from the FADC pulses is the ‘slope in time’ s_t for the drift direction x but a real geometric slope in wire direction y .

$$s_{x,u} = v_u s_{t,u} \approx s_{y,l} + \Delta s_l \quad (14)$$

$$s_{x,l} = v_l s_{t,l} \approx -s_{y,u} + \Delta s_u. \quad (15)$$

The terms Δs_l and Δs_u represent possible small misalignments between the two chambers (typically 1-2 mrad). Because most tracks are roughly vertical, a linear relation like above was considered sufficient for calibrating and correcting

such misalignments. Because the temperature and to some extent also the fraction of water vapour in the gas can be different in upper and lower chambers, separate drift velocities v_u and v_l for upper and lower chambers are calibrated and used for the track reconstruction. Figure 7 shows that the drift velocity correlates well with the temperature in the detector container but with a few hours delay. Remaining water vapour and perhaps other contaminations of the counting gas are the reason for this behaviour.

For the muon identification the spatial misalignment between upper and lower drift chamber has to be calibrated as well, in particular in the linear combination which is independent of the trigger delay.

To avoid selection effects in the calibration process, only events with a single track in the upper chamber and one in the lower chamber are used. A robust fit technique, minimizing the least absolute deviations rather than the usual least squares deviations, is applied for the fit of the drift velocity and slope misalignment. This kind of fit requires to keep the slopes of some 1000 track pairs in memory until enough data have been collected. The main advantage is that even with track pairs from air shower data – where random combinations of tracks in the two chambers are frequent – the proper drift velocity can be evaluated. For the final fit, obviously mismatching track pairs are discarded. The spatial misalignment is evaluated from the same data after discarding pairs inconsistent with the ‘average’ misalignment.

3.7 Calibration stability

Several thousand cosmic-ray events are required for each calibration step, with different calibration steps being processed in parallel during track reconstruction. Even at a maximum event rate of 50 Hz the calibration cycles are completed only every few minutes. During the measurements in the HEGRA array, with array triggers at a rate of some 10 Hz, where a detector has tracks in only one third of the events, the calibration cycles complete rather every 30 minutes. With fewer events per cycle the calibration period can be reduced – but at the cost of larger statistical errors of the calibration constants.

It has been carefully examined that the calibration algorithm is fast enough to take temperature dependent changes in calibration constants into account and precise enough to avoid that statistical calibration errors are a limiting factor for the track reconstruction accuracy.

For tests CRT detectors have been operated up to 30 days in a self-triggered mode with permanent online track reconstruction and self-calibration, recording all calibration and monitoring data. At the La Palma site, the temperatures measured in the detector container changed by up to 35 K during this 30 day period, with day-night variations up to 25 K above the iron plate and up to 14 K below the plate (fig. 7). Temperatures changed smoothly in the detector container due to the heavy iron plate although changes of up to 5 K/hour were observed in the morning. In the electronics box the temperature can change more rapidly during daytime because a fan is turned on at 25 °C and turned off at 20 °C.

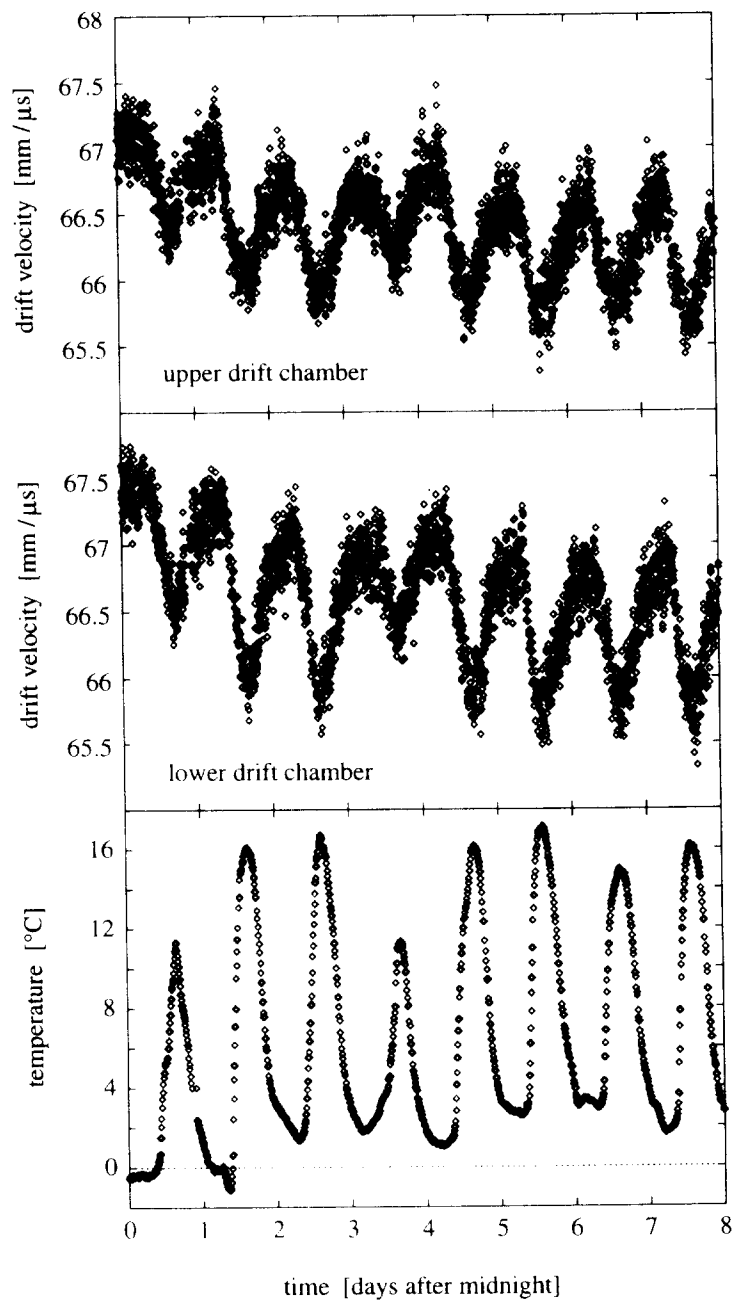


Figure 7: Drift velocities in upper and lower drift chambers and the average temperature in a CRT detector as functions of time.

However, the overall temperature changes in the electronics box are smaller than in the detector container.

One set of calibration parameters depending on the temperature in the electronics box are the FADC pedestals which varied by about 0.2 counts/K. This parameter set is determined at given intervals (typically every 10–30 seconds), independent of event data but causing some dead-time (typically 1%). Other electronic parameters like the voltages and currents were very stable.

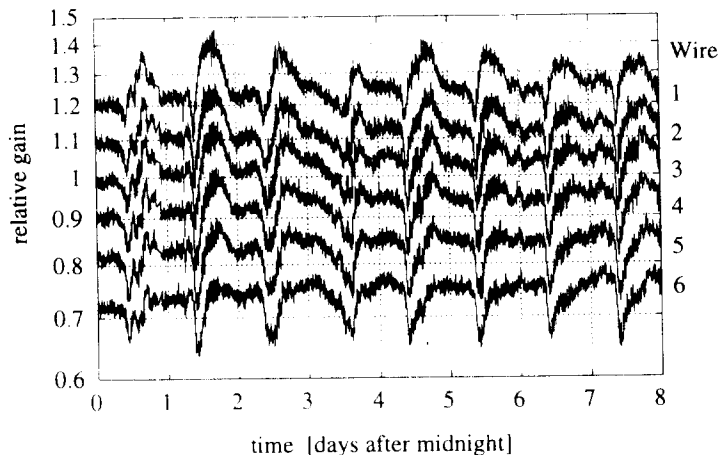


Figure 8: Relative gains of the wires of the upper drift chamber of a CRT detector as a function of time (suitably displaced to avoid overlaps). High-voltages were left constant.

Of the calibration parameters determined from event data, the gain factors show clear day-to-night variations (fig. 8). Because these variations are the same for all read-out channels of a wire and almost the same for all wires of a drift chamber, they are due to changes of the gas gain. These gain changes seem to be caused by density changes due to temperature gradients¹ and by contaminations in the gas. The parameters of interest, the gain ratios of the two sides of charge-division wires and of the four channels of the cathode pads, show no temperature dependence. Statistical fluctuations are more of concern for the gain ratios. Therefore, rather long calibration intervals are preferred for these ratios. Most coordinate calibration parameters also show only statistical fluctuations. One of the few parameter sets depending on temperature – by about 0.05 %/K – is that of the effective lengths of charge-division wires.

3.8 Test setups to study drift field distortions

An inhomogeneous drift field can result in systematic errors in the reconstruction of track angles. Such a field could be due to a mismatch in field cage potentials, due to mechanical tolerances, or due to surface or space charges. Although the drift cages of the CRT detectors were designed to avoid such problems as much as possible, two test setups were built to check for remaining inhomogeneities.

¹Because of the sealed container, the average gas density is independent of temperature. Temperature gradients, however, may induce local (in particular vertical) density gradients.

The first setup used an early drift chamber prototype and a N_2 laser with pulses of 1 ns duration and $14 \mu\text{J}$ energy. The laser beam ionized chemical additives in the chamber gas, resulting in a straight ‘track’ along the beam line. The only distortions found by this method were in the region where the drift cages were connected to the wire support structure. No signs of space or surface charge effects were found [7].

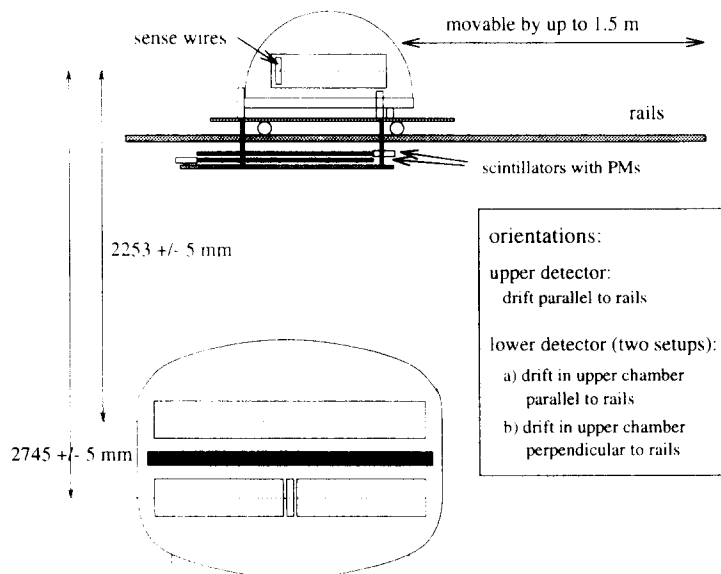


Figure 9: Test setup for field distortions with a movable small detector and scintillators on rails and a full-sized CRT detector below.

For the final CRT detectors a larger field-distortion test setup was built, using cosmic-ray muons (see fig. 9). For this purpose a smaller prototype detector with one rectangular drift chamber of $62 \times 60 \text{ cm}^2$ area was put on rails above the full-sized CRT detector to be tested. Two scintillators of 1 m^2 area with photomultiplier readout were used in coincidence to trigger on cosmic rays and to define the time of the particle passage in order to obtain actual drift distances of hits in the drift chambers. Calibration runs with internal-trigger operation of each detector were recorded between two measurement runs of up to 20 hours duration. Measurement runs were recorded in different positions of the small detector and with different orientations of the large detector. Both detectors were adjusted horizontally and the difference in height was carefully measured.

Events with at least one track in each detector were selected offline, tracks reconstructed and used for further analysis. Because temperature variations were small in the hall where the equipment was set up, drift velocities remained essentially constant during a measurement. The drift velocity in the small detector was derived from the histograms of pulse arrival times, which correspond to drift times of electron clouds up to 62 cm from the proportional wires. The velocity in the large detector was obtained from calibration run data as described in sect. 3.6.

Drift field distortions were searched by comparing *geometrical* slopes (as defined by the positions of tracks in the two detectors) with *reconstructed* slopes as

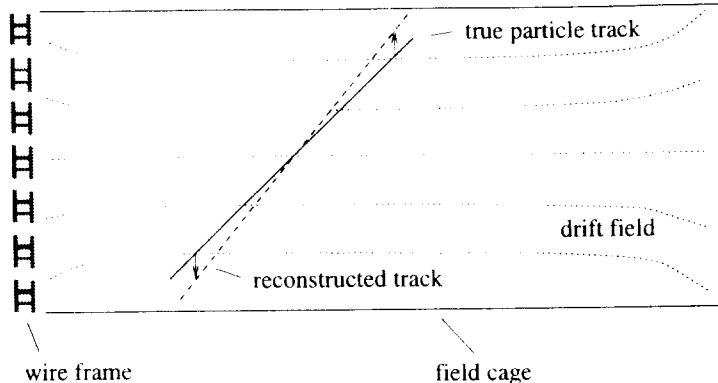


Figure 10: The field distortions found in CRT detectors (here severely exaggerated) lead to tracks reconstructed too close to vertical incidence.

functions of the track intersection position (or simply the drift distance) and the track slope. With this setup again small distortions were found near the wires and near the opposite sides of the field cages. The distortions (see fig. 10) result only in vertical displacements of the drifting electrons and not in a significant change of the drift distance. The distortions in the CRT detectors correspond to a *slope* ($\tan \theta$, with zenith angle θ) measured 3.2% too small for essentially all tracks, both in drift and wire direction projections. Because the arrangement of drift cages and wire support structure is the same for all CRT detectors, this systematic ‘imaging’ error can be easily corrected. Even a 1.0% error in the correction factor would, in fact, only result in a 0.1° angular error for a track with 10° zenith angle.

4 Monte-Carlo detector simulation

A detailed detector simulation by the Monte Carlo method has been implemented and used to check our understanding of the detectors and the main limitations for the angular resolution. The GEANT detector description and simulation tool [8] is used to trace the incident and any secondary particles through the detector, including scattering and interaction processes.

For all the charged particles crossing a *sensitive volume*, i.e. the 1 cm high cylindrical slices from where electrons can drift to the proportional wires, the various effects relevant to measured signals are simulated [9]. First of all, the fluctuations of the ionization along the track segments in the sensitive volumes are taken into account. This effect is responsible for the deterioration of the detector resolution with increasing zenith angle (see sect. 5.5). The longitudinal and transverse diffusion of the ionisation electrons on their way to the wires are included as well. At the sense wires the gas amplification is simulated, including the statistical fluctuations of the gain for each sample of electrons arriving at the wire and the $1/t$ time dependence of the signal.

The signals induced on the cathode pads in each time interval are based on an analytical approximation to the measured response function. The charge-division wire signals are also simulated. Because the wires are capacitively coupled to the

preamplifiers, the charge-division signals consist of a fast and a slow exponential component that influences the tails of the pulses. The slow component causes a slight undershoot on the ‘near’ side, where the fast component is larger, and a corresponding overshoot on the ‘far’ side. These effects are included in the simulation.

In order to obtain the proper frequency-dependent response function of the electronics chain of preamplifiers and shapers, the electronics was simulated with SPICE [10]. The resulting response function is folded with the charge at each preamplifier as a function of time. The electronics gains are chosen to have average pulse areas comparable to those measured with CRT detectors. The resulting signals are then digitized in 25 ns intervals as in the MPFA40 FADCs. Because the noise results from many different sources is very difficult to simulate, we decided to use measured noise signals and add them to the digitized simulated signals instead of adding simulated noise before the digitization.

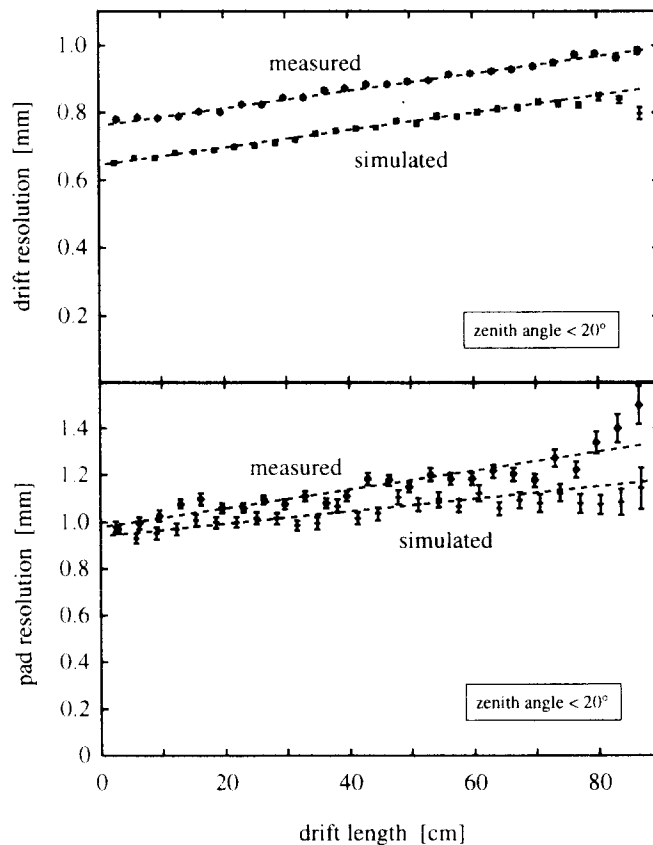


Figure 11: Simulated and measured resolutions in drift direction (top) and wire direction (pad resolution, bottom) for tracks with less than about 20° zenith angle.

The resulting ‘raw’ data are then processed by the same hit and track reconstruction software as used for the real data, and the same muon selection criteria are applied. In order to check the simulation procedure we compared pulse shapes, pulse-area histograms, and, in particular, the resolution with experimental data.

Indeed, simulated data behaves very much like real data, although the resolutions in drift as well as in wire direction are slightly (10–20%) better than in reality (see fig. 11). Due to the better charge-division resolution there are also less tracks with a bad reconstruction in the y - z plane as observed experimentally (see sect. 5.4).

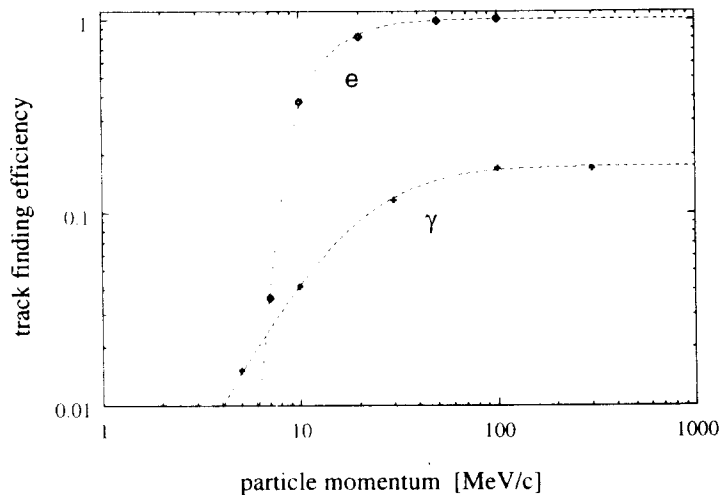


Figure 12: Simulated efficiency of reconstructing a track in the upper drift chamber as a function of the momenta of electrons and of gammas converting to e^+/e^- in the detector container. The dashed curves represent fits to the simulated efficiencies (points).

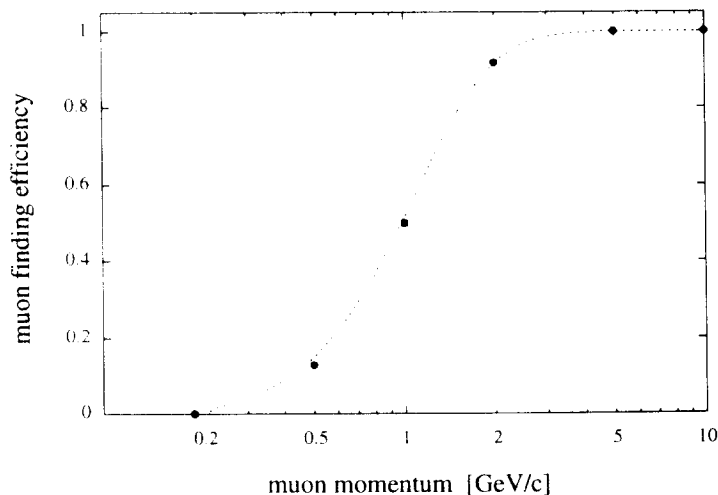


Figure 13: Simulated efficiency of reconstructing and identifying vertical muons. The dashed line is not a fit but a simple approximation accounting for losses due to multiple scattering in the iron plate, energy loss, and an internal resolution of 0.3° per chamber.

Understanding the resolution raises confidence in the simulations to attack questions which cannot be measured easily, like track reconstruction efficiencies as functions of particle types and momentum (see fig. 12 and 13) and the probabilities to misidentify electrons or hadrons as muons. The threshold for electron reconstruction is about 10 MeV/c. This can be explained by the energy loss in the

detector container (about 5 MeV) and the scattering of low-energy electrons in the counting gas which prevents reconstruction of straight tracks. Photons can also lead to reconstructed tracks if they suffer pair-production or Compton-scattering in the detector container or the drift cage.

The punch-through fraction of electrons misidentified as muons rises from 0.1% at 200 MeV/c to 0.6% at 500 MeV/c and 1.5% at 1 GeV/c, after applying the isolation criterium for tracks in the lower chamber. Without isolation criterium about three times more electrons would be identified as muons.

In addition, various sources of measurement errors, like diffusion or readout noise, can be switched on and off in the simulation. It turns out that for average tracks digitization, readout noise, diffusion, and ionization fluctuations along the tracks are of similar importance to the resolution in drift direction while the readout noise is the dominant contribution for the pad resolution.

5 Detector operation and performance

5.1 Operating CRTs with scintillator arrays

Operating CRT detectors together with a scintillator array was important to evaluate the performance of individual CRT detectors and of a small CRT array. CRTs have been operated at two scintillator arrays: the 25-station array on the Heidelberg institute campus at an altitude of 300 m [11] and the larger HEGRA array [12] on La Palma (Canary Islands) at an altitude of 2200 m. With the scintillator arrays, the secondary particle density in the shower can be sampled at more positions than with only 10 CRT detectors. Therefore, the shower core position can be better evaluated with scintillator data. Also the shower direction obtained from scintillator data can be used as a reference although the angular resolution of the HEGRA scintillator array is just of the same order as the resolution of a CRT detector for a single particle track. With the smaller Heidelberg scintillator array the array resolution is a severe limitation for observing the angular distribution of muons in air showers.

Simultaneous observations with a scintillator array and CRT detectors were used to check the particle angular distributions predicted by numerical air shower simulation programs, in particular by CORSIKA [13][14]. For measurements with the Heidelberg scintillator array and a first CRT prototype see [11]. Only data obtained with the HEGRA array and the 10 CRT modules on La Palma were used for the present paper. The HEGRA-plus-CRT observations were used to evaluate track reconstruction and muon identification efficiencies. We also looked for systematic ‘imaging’ errors of the CRT detectors with respect to the shower direction reconstructed from the HEGRA data although systematic reconstruction errors of a few tenths of a degree are expected also for the HEGRA scintillator array [12].

5.2 Operational conditions on La Palma

During most of the time since the first CRT detectors were installed on La Palma, the detectors were remotely operated from Heidelberg. The data backup was done

on Exabyte 8 mm data tape cartridges -- initially by local operators (mainly those of the HEGRA array) on La Palma and later remotely, using a 10-cartridges high-density tape drive with more than 50 gigabytes total capacity. With this tape drive local action was required only every three weeks to replace the tape cartridges. The online UNIX workstation was set up to reboot in case of power failures while all other online computers could be booted from the workstation, if necessary. Starting and controlling the data acquisition for individual CRT detectors or the whole CRT array was done from the UNIX workstation, a DECstation 5000/200.

A very slow deterioration of the gas quality was seen and the gas of the first four detectors was exchanged in November, 1993 -- up to 11 months after the initial filling. Five detectors have been opened on-site for repair of a particular badly soldered cable. The cause of this problem was identified and can be avoided in future detectors. Once a defective preamplifier had to be exchanged. Both types of defects caused only a slight deterioration of the angular resolution and the muon identification efficiency. In all cases the detectors remained fully operational. Except for these minor repairs the detectors performed without any problems, by now up to 24 months after installation on La Palma.

Because improvements of the track reconstruction software were still in progress after regular operation with HEGRA array trigger started in October, 1993, it was decided to record hit data for the first months and do the track reconstruction offline. Later-on the whole reconstruction was run online and only reconstructed tracks were recorded. Shower reconstruction is still done offline because the core location from the scintillator data is important for an array of only 10 CRT detectors.

5.3 Trigger and event rates

The trigger rate, event rates, and also the data rates of standalone CRT detectors as well as of the small CRT array on La Palma have been studied in detail. The peak event rate per detector is currently mainly limited by the CPU performance of the 25 MHz Motorola 68040 processors. For a 1 kHz single-detector trigger rate and full online pattern recognition and calibration an event rate of about 50 Hz is achieved with typically one track per event. This rate is perfectly adequate for the proposed large CRT array [2] where typically only 30-40 detectors out of almost 400 would be hit by charged secondaries from an air shower and, therefore, have a local trigger together with the common array trigger. With an array trigger rate of 100 Hz the rate relevant to the detector stations would range from some 20 Hz in the dense central part to less than 5 Hz in the outer part. At trigger rates below 20 Hz, e.g. the 8-15 Hz of the HEGRA array trigger, a dead-time fraction of about 1% is due to the FADC baseline calibration and about 2% due to processing of events. Rates of 100-200 Hz per detector seem feasible with more advanced but already available CPUs.

If only data of reconstructed tracks are transmitted to a central station, the overall amount is little more than 100 bytes per 'non-empty' event (i.e. with at least one track). Thus, the data rate transmitted to the central computer would even for a large CRT array with up to 400 detectors be within the bandwidth of standard

Ethernet if collisions on the cable are efficiently suppressed. Including calibration, monitoring, and auxiliary information a total data rate of some 700 kbytes per second are expected. After sorting of event data on the central computer and removal of redundant information like event numbers a rate of less than 500 kbytes per second would be obtained for further processing. With the present setup of 10 detectors and a 8 Hz detector trigger (17 Hz global trigger) about 10 kbytes are recorded per second.

Internal trigger rates were found to be significantly higher than expected from [15], which is based on [16]. At the the institute campus in Heidelberg (300 m a.s.l.), instead of the expected rate of some 450 Hz the observed rate for 3 out of 4 wires of the upper chamber is about 790 ± 40 Hz with 0.94 ± 0.03 tracks reconstructed per event. The reason for this discrepancy seems to be the low threshold of CRT detectors for the soft e^\pm component of secondary cosmic rays.

When looking for muons, no obvious discrepancy is found. The expected rate, including the geometric detector acceptance, is about 250 Hz. A CRT muon trigger rate of 330 Hz is observed. With this trigger 0.55 muons were reconstructed per event (corresponding to a 182 Hz muon rate), if the same muon identification criteria as for shower muons are applied. If less strict criteria are applied, which are more appropriate for the softer non-shower muons, 0.65 muons per event (corresponding to 215 Hz) are found. Even with the less strict muon cuts a significant fraction (about 10-20%) of the soft non-shower muons are expected to fail the cuts. Expected and measured muon rates are, therefore, consistent. For a CRT detector in Heidelberg rather 35% instead of the quoted 75% [15] of the observed particle flux is due to the muon component.

At mountain altitude (La Palma, 2200 m a.s.l.), the fraction of the soft component is even larger. For the same detector and the same operating conditions the trigger rates of single wires in the upper drift chamber and of coincidences rise by 37% with respect to the values measured at Heidelberg. Rates in the lower chamber increase by only 20%. Muon trigger rates increase by 32%.

For a CRT array triggered on coincidences between CRT detectors, coincidence gate widths of at least the maximum drift time – some $14 \mu\text{s}$ – are required. With these widths and an ordinary majority trigger logic, random array triggers can be a serious problem. Assume that in an array with n detectors used for the trigger logic all detectors have the same (independent) single-detector rate ν_1 . If at least k out of the n detectors are required for a coincidence of width τ , the random array trigger rate is

$$\nu_{k,n}^* = k \binom{n}{k} \nu_1 (\nu_1 \tau)^{k-1}, \quad (16)$$

without taking into account that the trigger gate causes a dead-time τ after each trigger. Correcting for that, the random rate is

$$\nu_{k,n} = \nu_{k,n}^* \exp(-\tau \nu_{k,n}^*). \quad (17)$$

Measured trigger rates and expected random rates for the small array on La Palma are shown in table 1. With the small array a trigger of at least four out of eight detectors is required to have the random rate well below the measured rate.

Table 1: Trigger rates for the small CRT array at La Palma with eight detectors connected to the central trigger logic. In addition to measured trigger rates the expected random trigger rates for the average single-rate of 1019 ± 8 Hz and a gate width of $15\ \mu\text{s}$ are shown. The CRT detectors were triggered with a coincidence of at least 3 out of 4 wires in the upper chambers.

trigger multiplicity (k of n)	Measured trigger rate [Hz]	Expected random rate [Hz]
≥ 1 of 8	7280 ± 8	7215 ± 50
≥ 2 of 8	848 ± 5	861 ± 13
≥ 3 of 8	56.5 ± 0.8	40.0 ± 0.9
≥ 4 of 8	8.1 ± 0.4	1.02 ± 0.03
≥ 5 of 8	3.8 ± 0.2	0.016 ± 0.001
≥ 6 of 8	2.3 ± 0.15	10^{-4}
≥ 7 of 8	1.23 ± 0.06	10^{-6}
all 8	0.84 ± 0.06	10^{-9}

If the 200 central detectors of a large CRT array were used for the trigger, then with $\tau = 15\ \mu\text{s}$ and an expected single-rate (at an altitude near 4000 m) of $\nu_1 = 1600$ Hz, at least 20 detectors would be required for a clean array trigger without a significant number of random triggers. With a trigger scheme looking for clusters of triggering detectors this threshold could be considerably reduced. Nevertheless, in any event of the order of $\tau\nu_1 = 2.4\%$ of all detectors would be hit by cosmic ray secondaries which are not from the shower that triggered the array.

Most of these random tracks could be safely discarded during data processing because they are generally far from the shower core and not correlated with the shower direction. In particular, random muon tracks can be recognized very well due to the narrower intrinsic angular distribution and the fact that the time when the particle passed the detector can be reconstructed from the track pair. For electrons, however, a significant but acceptable probability to have random tracks remains.

5.4 Track reconstruction and muon identification efficiencies

The track reconstruction efficiencies for data taken with the HEGRA trigger on La Palma has been evaluated. Unless otherwise stated, the mentioned efficiencies apply to detectors with four cathode-pads boards per drift chamber triggered by the HEGRA array. Note that the efficiencies depend on particle energy and type, track multiplicities, on the position in a chamber, and on the zenith angle. Muons and other high-energetic particles penetrate the gas in a drift chamber with very little scattering. On the other hand, low-energy particles – mainly electrons – may scatter quite significantly or even stop within a drift chamber. In addition, the detector response deteriorates if the detector is hit by many particles in the same event.

The overall detector efficiency can be expressed by the *effective area*, which is the measured rate divided by the flux of particles from a given direction. In a simplified way the effective area of a CRT for reconstructing a track with m hits from a charged particle of zenith angle θ can be expressed as

$$A_{\text{eff},m} = \sum_{k=m}^6 \sum_{l=m}^k A_{\text{geo},k} \epsilon_{\text{hit},l(k)} \epsilon_{x,m(l)} \epsilon_{y,m} \cos \theta. \quad (18)$$

$A_{\text{geo},k}$ is the horizontal geometrical area for particles passing through the chamber such that they should produce k hits under ideal circumstances (averaged over all azimuth angles). Usually, ideal tracks should have six hits, but near the circular outer border or when tracks cross the wire ‘plane’ less hits are found (see fig. 14). $\epsilon_{\text{hit},l(k)}$ is the efficiency of finding l out of the k possible hits, $\epsilon_{x,m(l)}$ that of finding a sufficiently straight track with m of the l hits in the first reconstruction step (in the x - z plane), and $\epsilon_{y,m}$ that of reconstructing this track also in the second projection (the y - z plane). Averaged over all hit numbers the previous equation can be rewritten:

$$A_{\text{eff}} = A_{\text{geo}} \epsilon_{\text{hit}} \epsilon_x \epsilon_y \cos \theta. \quad (19)$$

For muons, where tracks in both chambers are required, the geometrical area $A_{\text{geo},\mu}$ is different from that for tracks in a single chamber. Including the muon selection cuts a simple expression for the effective muon reconstruction area is

$$A_{\text{eff},\mu} = A_{\text{geo},\mu} (\epsilon_{\text{hit}} \epsilon_x \epsilon_y)^2 \epsilon_{\text{angle}} \epsilon_{\text{pos}} \epsilon_{\text{iso}} \cos \theta. \quad (20)$$

Here, ϵ_{angle} is the efficiency that the angles of the two tracks match, ϵ_{pos} that the extrapolated positions at the middle of the iron plate match, and ϵ_{iso} that the muon track in the lower chamber is isolated.

Table 2: Sensitive horizontal geometrical detector areas A_{geo} (in m^2) as a function of zenith angle θ after applying the geometrical acceptance for tracks in the upper chamber (with at least 4, 5, or 6 hits) and for muons.

track type	$\theta = 0^\circ$	30°	45°	60°
≥ 4 hits	2.54	2.44	2.35	2.21
≥ 5 hits	2.54	2.34	2.13	1.94
6 hits	2.54	2.21	1.97	1.57
muons	2.54	1.95	1.53	0.89

While geometrical areas are easily calculated (see table 2) the efficiency factors are derived from the cosmic ray data. Efficiencies for high-energetic secondaries with little scattering in a drift chamber can be obtained from muon tracks. The hit efficiency ϵ_{hit} is evaluated from muon tracks in a fiducial volume of the drift chambers away from the edges and wire plane, where in the ideal case only 6-hit tracks are expected. Hit losses can be due to ionization fluctuations or due to overlapping multiple pulses. In the case of ionization fluctuations with probability p to find a single hit, the probabilities for finding 6, 5, or 4 out of 6 possible hits are $\epsilon_{x,6(6)} = p^6$, $\epsilon_{x,5(6)} = 6p^5(1-p)$, and $\epsilon_{x,4(6)} = 15p^4(1-p)^2$, respectively. Observed

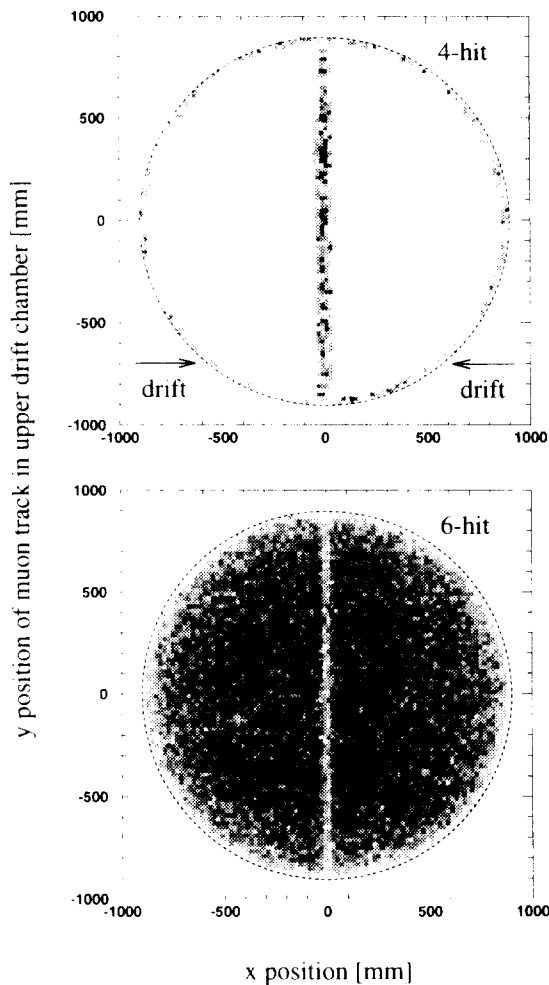


Figure 14: Histograms of muon track positions in the upper drift chamber, for tracks with four hits and with six hits. Four-hit tracks are predominantly found for particles crossing the wire plane or the outer edge. The outer detector border is indicated by dashed circles.

fractions of single muon tracks in the fiducial regions are 95%, 5%, and 0.2%, both in the upper and the lower chambers. The corresponding single hit efficiency p is 99.1%. Losses of tracks due to ionization fluctuations, i.e. having only three hits or less, are negligible. However, the track finding may be disturbed by additional tracks. The fraction of 4-hit muon tracks rises to 1.4% with one other track, 3.2% with two, and 4% with three other tracks. The average of all events is 1.4%. Muon tracks actually lost due to other tracks are estimated to be less than 0.5% per chamber.

For high-energetic particles like the muons no significant losses due to scattering in the drift chamber gas are expected ($\epsilon_x \approx 1$). However, a low-energy particle scattering in the gas may be reconstructed e.g. as a 4-hit track because the hits on two wires are not on a sufficiently straight line with the four others. Due to such low-energy particles, the overall fraction of 4-hit tracks is much larger than

for muons. With only one track in a drift chamber, the fractions of 6-, 5-, and 4-hit tracks are 70%, 16%, and 14% for the upper chamber and 54%, 21%, and 25% in the lower chamber. With more than one track, the fraction of 4-hit and 5-hit tracks is even larger.

A significant fraction of the 4-hit tracks cannot be properly reconstructed in the y - z projection, e.g. because they have no or too small hits on the two charge-division wires. The efficiency $\epsilon_{y,4}$ for proper y - z reconstruction of 4-hit tracks falls from 90% for almost vertical tracks (in the x - z plane) to 88% for tracks at 50° projected zenith angle (averaged over all track multiplicities). For 5-hit tracks $\epsilon_{y,5}$ rises from 97% for almost vertical tracks to 99% at 50° and for 6-hit tracks $\epsilon_{y,6}$ rises from 99.4% at 0° to 99.8% at 50° . With no or few other tracks in a chamber, the efficiencies are much better: with three or less tracks in a chamber $\epsilon_{y,6}=99.9\%$, $\epsilon_{y,5}=99.8\%$, and $\epsilon_{y,4}=91.4\%$, averaged over all angles. The performance of detectors with only three cathode-pads boards per chamber is slightly worse. Assuming that the same hit- and multiplicity-dependent numbers apply for muons as for all other particles, the overall y - z reconstruction efficiency for muons is about 99.6% in each chamber. Other possible reconstruction errors like reconstruction into the wrong drift cage (mirror tracks) or completely wrong reconstruction in y z are, at least for 5- and 6-hit tracks, very unlikely and insignificant.

The 4-hit tracks are not just badly reconstructed tracks. They are mainly from low-energy particles which have a rather poor angular correlation with the shower axis, i.e. the primary cosmic ray, anyway. Therefore, 4-hit electron tracks can essentially be ignored when reconstructing the shower directions from tracks in an array of CRT detectors.

The muon-specific efficiency factors ϵ_{angle} , ϵ_{pos} , and ϵ_{iso} are calculated by releasing one cut and looking at the distribution in the corresponding variable. Because the trigger delay is not known online, the position cut is done with linear combinations of the two coordinates: ρ_1 which is independent of the delay and ρ_2 which is only available offline after subtraction of the average delay (see sect. 2.5). All muons should have $\rho_1 \approx 0$, shower muons also $\rho_2 \approx 0$.

See fig. 15 and fig. 21 for the observed angular match and fig. 16 for the distribution of the position parameters ρ_1 and ρ_2 . For a $2.5^\circ \times 2.5^\circ$ angular cut ϵ_{angle} is $93.5 \pm 1.2\%$ for CRTs placed inside the HEGRA array and triggered by HEGRA showers. The losses are consistent with the multiple scattering of the muons in the iron plate. Muons lost in the angular cut essentially all have momenta less than $2 \text{ GeV}/c$.

In fig. 16 it turns out that in a fraction of the events, the charge-division coordinates were wrong by one or even more pad periods. Most such events have additional tracks in the detector which disturbed the track reconstruction. On average, 87% of all shower muons are found in the central peak ($|\rho_1| < 30 \text{ mm}$ and $|\rho_2| < 50 \text{ mm}$), 10% in the four peaks corresponding to an offset of one pad period, and 2.5% in further peaks (97%, 2.6%, and 0.2% in events with no other tracks than the muon). For this reason, track pairs in the one-period-offset peaks are, generally, also accepted as muons ($\epsilon_{\text{pos}}=97.5\%$).

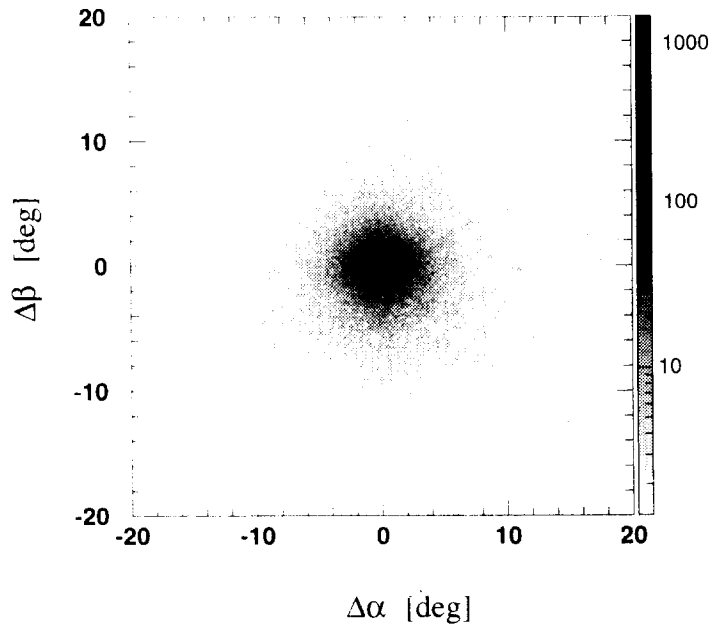


Figure 15: Histogram of the angles between all pairs of a track in the upper chamber and one in the lower chamber after applying the ρ_1 cut. Tails of the distribution are enhanced by the logarithmic grey-scale.

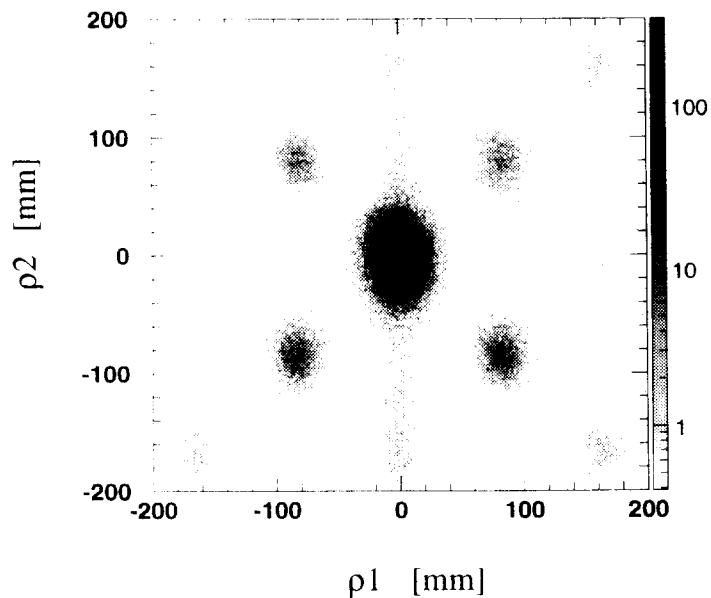


Figure 16: Histogram of the muon cut parameters ρ_1 and ρ_2 for the separation between extrapolated upper and lower track in the iron plate. Note the logarithmic grey-scale to enhance faint details. The central peak is from correctly reconstructed shower muons, the other peaks from muon tracks reconstructed with the correct angle but offset by one or more pad periods. The vertical strip in the middle is from accidental muons not originating from the shower.

In a final cut, candidates for punch-through electrons are discarded. From showers of high-energy electrons in the iron plate sometimes one or several tracks may leak into the lower drift chamber, resulting in fake muons. Hadrons interacting in the iron plate could also cause more than one track in the lower chamber. For 7.7% of all shower-muon candidates a second track is found within an extrapolated intersection in the iron plate less than 60 mm in drift projection from the muon track (8.3% if the one-period-offset peaks are included). Of these 1.6% (1.9%) are expected to be real shower muons with an accidental second track, i.e. $\epsilon_{\text{iso}} = 98.4\%$ (98.1%). The other 6.1% (6.4%) are punch-through electrons or interacting hadrons. According to detector simulations, about 68% of punch-through electrons are recognized as such. Thus, about 3% of the muon candidates with HEGRA trigger should be unidentified punch-through electrons with just one track in the lower chamber, assuming that all identified punch-through particles are electrons. That corresponds to about $7 \cdot 10^{-4}$ of the total number of registered electrons. According to shower simulations, most of these high-energy electrons are very close (< 25 m) to the shower core. Beyond 50 m from the core the punch-through electrons and hadrons should be insignificant. In the HEGRA-triggered data, the ratio of identified punch-throughs to muons drops from 9% at 20 m core distance to 3% at 250 m.

Apart from the geometrical acceptance, the overall efficiency for muons in HEGRA-triggered showers is $87 \pm 3\%$ if the one-period-offset peaks in the ρ_1 - ρ_2 plot are included, $78 \pm 4\%$ if only the central peak is used. For the detectors with only three cathode-pads boards per drift chamber $84 \pm 4\%$ of the muons ($74 \pm 5\%$ without offset peaks) are found. For muons above 2 GeV/c, which have negligible losses due to the angle cuts, the efficiency is 92% with offset peaks and four cathode-pads boards. The remaining background among the shower muon candidates is estimated as up to 3% single-track punch-through electrons, 1.2% non-shower muons and 0.2% random combinations of tracks in upper and lower chamber (0.08% with the central ρ_1 - ρ_2 peak only). Very close to the shower axis several percent are expected to be hadrons.

5.5 Track resolution

The angular resolution of the CRT detectors for particle tracks has been measured in several different ways. Each method has its advantages and its drawbacks. Three methods are shown here in detail:

Method 1: Measure the residuals of track fits in both drift and wire directions and determine the corresponding angular resolutions. The advantage of this method is that it can be applied after collecting just a few thousand events with internal trigger. The drawbacks are that it does not take drift field distortions into account and that, strictly speaking, with weighted fits – where weights are determined by signal amplitudes, overflows, too large pulse widths, the distance to the next hit and so on – the corresponding angular resolution has to be determined by a detector simulation including details of the detector. A simple application of this method is only useful for a first estimate of the resolution that can be expected.

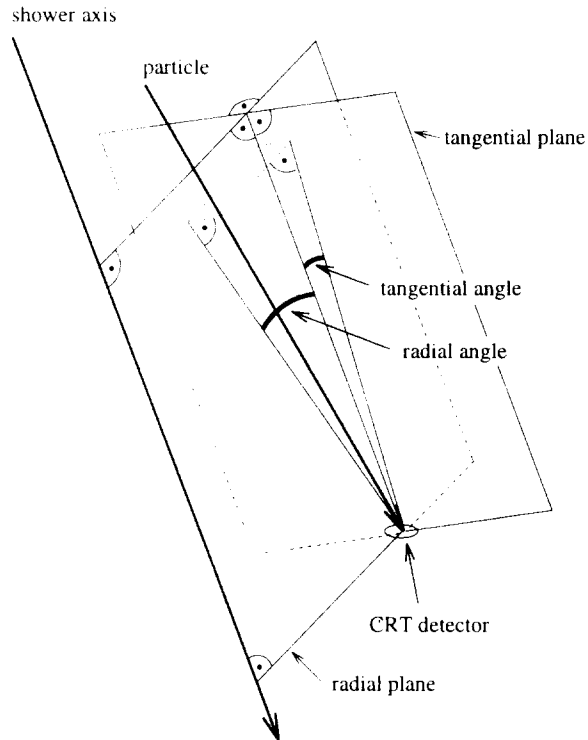


Figure 17: The geometry of radial and tangential angles between the shower axis, e.g. as reconstructed from scintillator data, and the track of a particle measured by a CRT detector.

Method 2: Measure the angle between the tracks of muons in upper and lower chamber. The distribution of muon angle differences accounts not only for twice the angular resolution in a drift chamber but also for multiple scattering of the muons in the iron plate. In general, the scattering contribution to the angle difference distribution cannot be unfolded reliably, because the momentum distribution of the registered muons is not accurately known and scattering angles are of the same order as the resolution. This method is more accurate when muons in extended air showers are used instead of muons seen with CRT detectors in stand-alone operation, because EAS muons less than 100 m from the shower core have a much larger average momentum. The advantage of the method is that the effects of possible drift field irregularities are included. However, the resolution determined this way does not include systematic reconstruction errors in both drift and wire direction as discussed in sect. 3.8.

Method 3: Measure the angle between CRT muon tracks and the corresponding reconstructed shower axis from scintillator data. This method has several advantages. Measurements of CRT detectors and scintillator array are completely independent (except for the trigger). Therefore, systematic deviations of CRT tracks with respect to the reconstructed shower axis can be measured. Due to the large intrinsic scatter of the *radial* angles, only the *tangential* component (angle difference in a plane parallel to the shower axis and perpendicular to the shortest

line from the CRT detector to the shower axis, see fig. 17) with an intrinsic width of only some 0.2° should be used. For this decomposition the shower core position from the scintillator data is needed.

By method 1 the dependence of the hit resolution on various parameters has been evaluated, in drift (x) as well as in wire (y) direction. The hit resolutions in both directions show a linear dependence on the drift length (fig. 18). The resolution in x also depends on the track angle in the x - z plane and that in y on the angle in the y - z plane (fig. 19) but not vice-versa. In addition, the pad and charge-division resolutions but not the x resolution have been found to deteriorate with an increasing number of tracks in the drift chambers (see fig. 20). This deterioration is mainly due to the slow signal components which slightly offset the FADC pedestals for subsequent hits. The hit resolutions averaged over all angles, drift distances, and track multiplicities are about 0.9 mm in x and 1.1 mm in y , corresponding to track angle resolutions of 0.31° and 0.43° with unweighted track fits. The weighted fits, as implemented, should be 10–15% better.

The projected angles between the upper and lower tracks of shower muons (fig. 21, see also fig. 15) include the resolution in x of one chamber, in y of the other, and the multiple scattering in the iron plate. The observed Gaussian σ of 0.57° is consistent with the resolution derived from the fit residuals, if the average multiple scattering of muons with a typical momentum of the order of 10 GeV/ c is taken into account. Therefore, irregular drift field distortions do not pose a significant limitation on the resolution of the CRT detectors. For muons observed with standalone CRT detectors the average angles between the two tracks are 40% larger due to the lower muon momentum and the larger scattering in the iron.

The expected angular resolution for a single shower muon is expected to be of the order of 0.4° in both projections if systematic field distortions (sect. 3.8) are also insignificant or can be fully corrected afterwards.

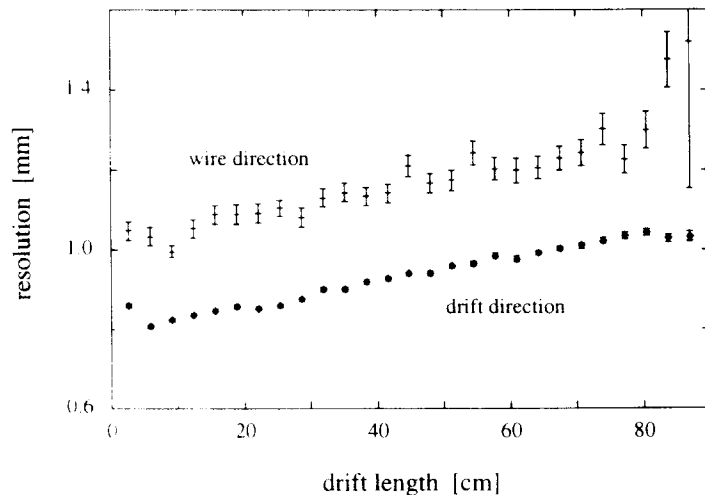


Figure 18: Dependence of the hit resolutions as functions of the drift length, averaged over all angles and multiplicities.

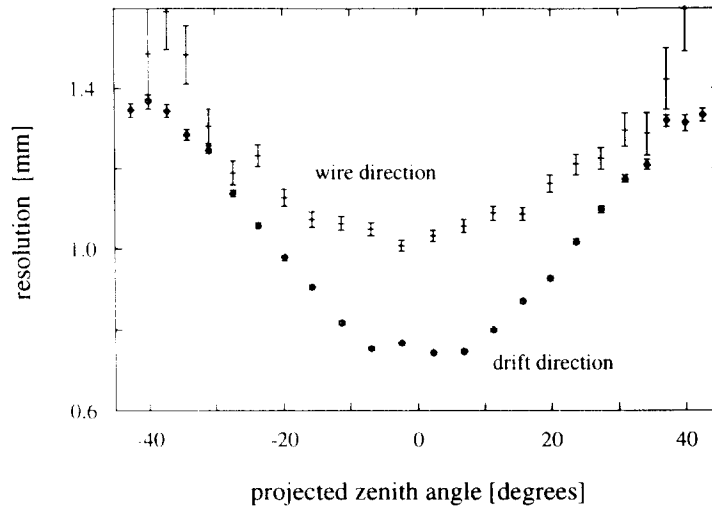


Figure 19: Hit resolution in x as a function of the angle in the x - z plane and the resolution in y as a function of the angle in the y - z plane, averaged over all drift distances and multiplicities.

By comparison with the HEGRA shower axis, the muon angular resolution has been checked. For this comparison the inclinations of the detectors and scaling factors for the track slopes have been evaluated by comparison with HEGRA data. A small systematic mismatch of a few tenths of a degree between these inclinations and those determined with standalone CRT detectors could be either due to HEGRA or to the east-west effect caused by the earth's magnetic field. The track-slope scales generally deviate by less than 1% from the nominal value.

Fig. 22 shows the distribution of the tangential angle difference between single

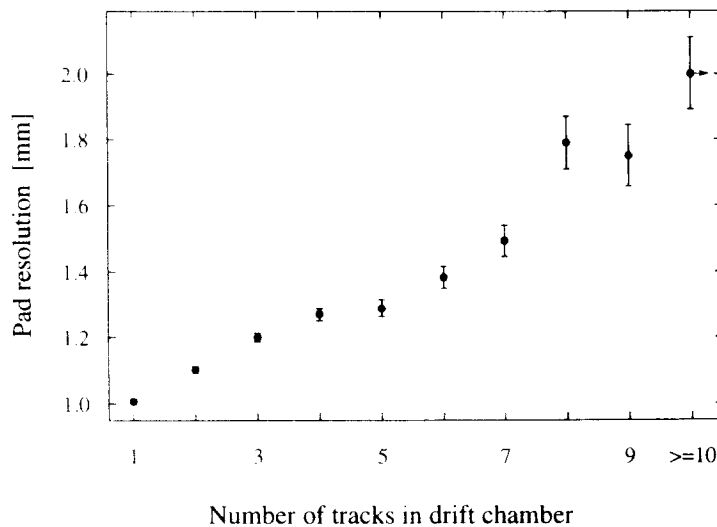


Figure 20: The cathode-pad resolution as a function of the number of tracks in the drift chamber.

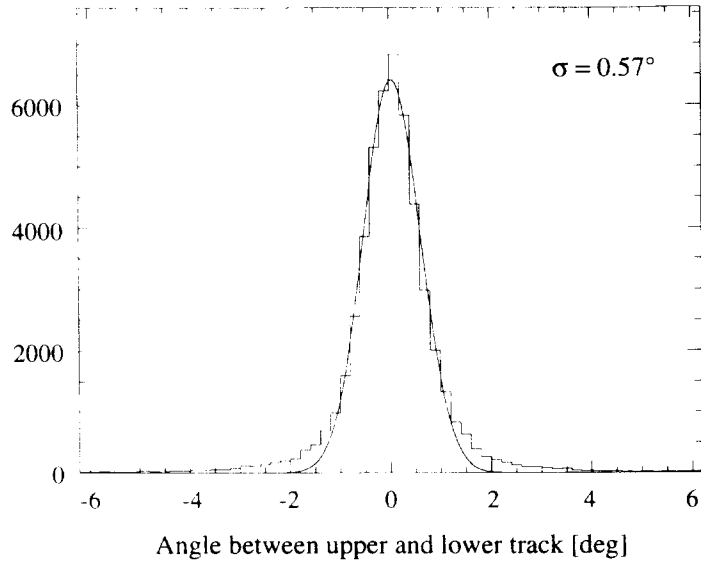


Figure 21: The projected angles between upper and lower tracks of muons in HEGRA-triggered showers.

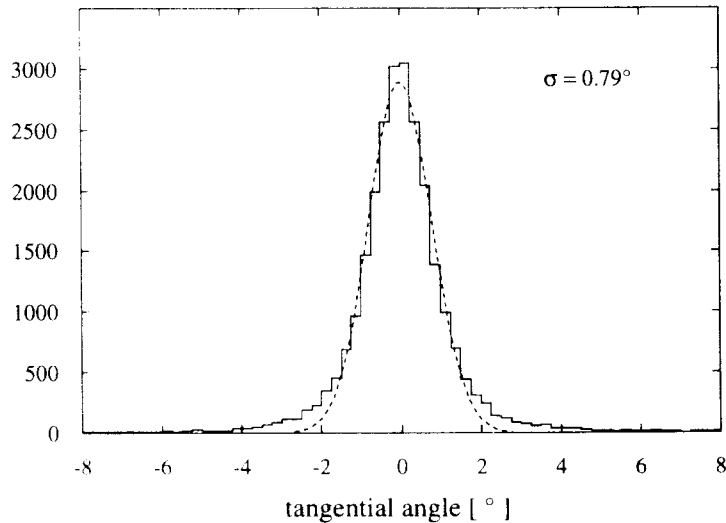


Figure 22: The distribution of tangential angles between single muons in CRT detectors and showers reconstructed from the HEGRA scintillator array.

muon tracks and the shower axis obtained from the HEGRA scintillator data. The achieved resolution of 0.79° is, in fact, mainly due to the HEGRA resolution. The HEGRA resolution improves with increasing shower size while the CRT muon resolution is essentially independent of the shower size. Due to an increasing number of other tracks in addition to the muon, the CRT muon resolution could only deteriorate with increasing shower size. Indeed, the tangential angle difference resolution improves with increasing shower size (see fig. 23) to about $0.4\text{--}0.5^\circ$ for very large showers. We conclude that CRT detectors have a resolution of about 0.4° for single muons, when systematic offsets from the HEGRA reference system

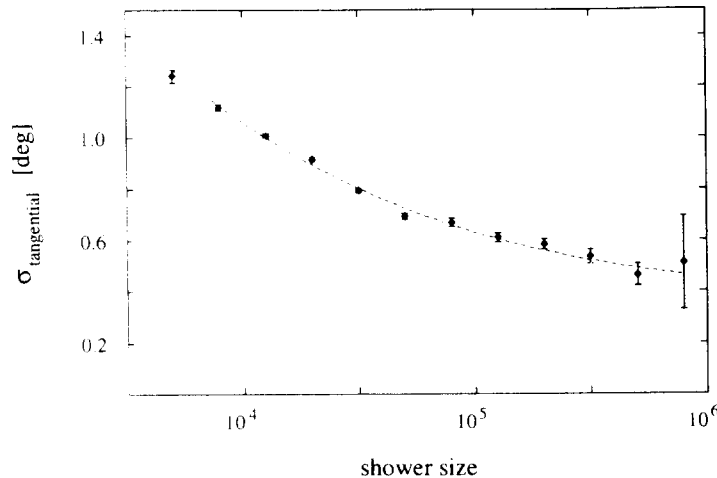


Figure 23: The resolution of tangential angles between CRT muons and HEGRA showers as a function of shower size N_s . The dashed line is a fit, assuming a size-independent CRT resolution and a HEGRA resolution proportional to a power of N_s .

are corrected for.

The angular resolution has also been checked using the angles between two muons in the same detector as well as in separate detectors and by data obtained with a trigger from an Atmospheric Cherenkov Telescope on the HEGRA site. Results from these methods are consistent with those of the methods explained in detail.

6 Conclusions

The operational experience of up to two years with the 10 CRT detectors on La Palma at an altitude of 2200 m has shown that CRT detectors are very robust devices. With these detectors the TPC technique has been adopted to outdoor mountain-altitude conditions. The detectors have been operated with full online data processing and detector calibration at the local detector stations. Processing speeds with the current Motorola 68040 CPUs are fully sufficient for the 10 CRT detectors operated either with triggers from the HEGRA array or as a small array on its own. Processing speeds would also be adequate for a large CRT array as proposed by [2].

Using CRT detectors, tracks from electrons above about 10 MeV energy can be reconstructed and muons above about 1 GeV can be identified very well. Punch-through electrons are efficiently suppressed and occasional random muons not related with the measured showers are recognized. Muons are very rare in γ -ray initiated air showers. Therefore, a single shower muon would be sufficient to reject a hadron shower with a large CRT array searching for sources of cosmic γ -rays above a few TeV energy.

The achieved angular resolution is about 0.4° for muons. For high-energy electrons the resolution is comparable to that while for low-energy electrons (below

about 100 MeV) the resolution is somewhat deteriorated by multiple scattering in the detector container. The good overall angular correlation of the shower secondaries with the direction of the primary cosmic rays is conserved. We estimate that with a large CRT array the direction of the primaries can be determined with an accuracy of about $(3^\circ-4^\circ)/\sqrt{N}$ where N is the number of recorded secondaries in the CRT detectors. A detailed study of the resolution to be achieved with a CRT array is still in progress.

Acknowledgments

We would like to thank the members of the HEGRA collaboration for their help during buildup and operation of the CRT detectors on La Palma and for providing the shower data of the scintillator array.

References

- [1] J. Heintze et al., Cosmic Ray Tracking – ein neuer Weg für die γ -Astronomie bei hohen Energien, Proposal, 1988.
- [2] J. Heintze et al., Nucl. Instr. and Meth. A277 (1989) 29.
- [3] M. Feuerstack et al., Addendum to the proposal 'Cosmic Ray Tracking – a new approach to high-energy γ -astronomy', 1990.
- [4] K. Bernlöhr et al., The Cosmic Ray Tracking detector system, submitted to Nucl. Instr. and Meth. A, 1995 (Paper I).
- [5] V. Matheis, PhD thesis, Heidelberg, 1994.
- [6] G. Leffers, Diploma thesis, Heidelberg, 1992.
- [7] V. Matheis, Diploma thesis, Heidelberg, 1991.
- [8] GEANT - Detector Description and Simulation Tool, CERN, Program Library Office, Geneva, 1993.
- [9] R. Zink, PhD thesis, Heidelberg, 1995.
- [10] T. L. Quarles, SPICE3 User's Guide, Department of Electrical Engineering and Computer Sciences, University of California, Berkeley, 1989.
- [11] S. Gamp et al., Phys. Rev. D46 (1992) 2831.
- [12] F. Aharonian et al., Proc. of 23rd Intern. Cosmic Ray Conf., Vol. 4, p. 291, Calgary, 1993.
- [13] J. N. Capdevielle et al., The Karlsruhe Extensive Air Shower Simulation Code CORSIKA, Technical Report KfK 4998, Institut für Kernphysik, Kernforschungszentrum Karlsruhe, 1992.
- [14] J. Knapp and D. Heck, Extensive Air Shower Simulation with CORSIKA: A User's Manual, Kernforschungszentrum Karlsruhe and Universität Karlsruhe, 1994.
- [15] Particle Data Group et al., Phys. Rev. D50 (1994) 1173.
- [16] B. Rossi, Rev. Mod. Phys. 20 (1948) 537.